UNIVERSIDADE FEDERAL DO RIO DE JANEIRO
INSTITUTO DE MATEMÁTICA
CURSO DE BACHARELADO EM CIÊNCIA DA COMPUTAÇÃO

FLAVIO MEDEIROS RANGEL

COMPARING NUMERICAL METHODS TO CALCULATE FLUID PRESSURE

RIO DE JANEIRO
2020

FLAVIO MEDEIROS RANGEL

COMPARING NUMERICAL METHODS TO CALCULATE FLUID PRESSURE

Trabalho de conclusão de curso de graduação
apresentado ao Departamento de Ciência da
Computação da Universidade Federal do Rio
de Janeiro como parte dos requisitos para
obtenção do grau de Bacharel em Ciência da
Computação.

Orientadora: Profa. Juliana Vianna Valério

RIO DE JANEIRO

2020
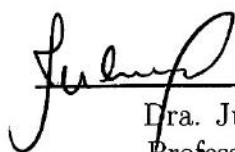
CIP - Catalogação na Publicação

FLAVIO MEDEIROS RANGEL

COMPARING NUMERICAL METHODS TO CALCULATE FLUID PRESSURE

> Trabalho de conclusão de curso de graduação apresentado ao Departamento de Ciência da Computação da Universidade Federal do Rio de Janeiro como parte dos requisitos para obtenção do grau de Bacharel em Ciência da Computação.

Aprovado em 03 de ___marco___ de 2020

BANCA EXAMINADORA:

_____
Dra. Juliana Vianna Valério
Professora Adjunta (UFRJ)

_____
Dr. Thiago Gamboa Ritto
Professor Adjunto (UFRJ)

_____
Dr. Marcello Goulart Teixeira
Professor Adjunto (UFRJ)

ACKNOWLEDGEMENTS

RESUMO

O presente trabalho teve por objetivo comparar o método de elementos finitos com o método de diferenças finitas no cálculo numérico da pressão interna do mancal com excentricidade e geometria cilíndrica, com uso da geometria para simplificação da equação de Navier-Stokes. Fez-se o uso do software de código aberto ROSS para prover os resultados com o método de diferenças finitas, enquanto que o método de elementos finitos foi programado pelo autor. Como base para checagem de erro, fez-se o uso de soluções não numéricas para o problema do mancal nos casos curto e longo, onde a equação de Navier-Stokes torna-se ainda mais simples. Avaliou-se o número de iterações até conversão da malha bem como o tempo de processamento de cada iteração. Os resultados indicaram um desempenho levemente superior do método de diferenças finitas para o cenário e os critérios avaliado e considerando diferentes configurações da malha.

Palavras-chave: cálculo numérico. máquinas rotativas. equação de Poisson.

ABSTRACT

The present work aimed to compare the finite-element method with the finite-difference method in the numerical calculation of the internal pressure of the bearing with eccentricity and cylindrical geometry, using its geometry to simplify the Navier-Stokes equation. The open-source software ROSS was used to provide the results for the finite-difference method, while the finite-element method was programmed by the author. As a basis for error checking, non-numerical solutions were used for the bearing problem in short and long cases, where the Navier-Stokes equation becomes even simpler. The number of iterations until mesh conversion was evaluated, as well as the processing time of each iteration. The results indicated a slightly superior performance of the finite-difference method for the scenario and the evaluated criteria and considering different mesh configurations.

Keywords: numerical analysis. rotating machines. Poisson's equation.

LIST OF FIGURES

LIST OF TABLES

LIST OF ABBREVIATIONS AND ACRONYMS

Eq.   Equation

Fig.   Figure

ROSS   Rotordynamic Open Source Software

FDM   Finite-difference method

FEM   Finite-element method

LIST OF SYMBOLS

ρ	Fluid's density in mass per volume
$\vec{P}$	Linear momentum of a system
$\vec{v}$	Velocity vector in the velocity field
σ	Cauchy stress tensor
μ	Fluid viscosity
p	Pressure
R_o	Radius of the outer cylinder
R_i	Radius of the inner cylinder
ρ	The fluid's density
θ	Angle from the tangential-axis
α	Constant of the simplified Navier-Stokes equation
β	Constant of the simplified Navier-Stokes equation
γ	Constant of the simplified Navier-Stokes equation
P_{in}	Pressure that enters the bearing
P_{out}	Pressure that leaves the bearing
N_Z	Number of mesh points in axial direction
N_θ	Number of mesh points in azimuthal direction
ω	Angular frequency
ϕ	Approximation of p using basis functions
φ_i	A basis function
κ	A weighting function
Ω	The region over a 2-dimensional space
Γ	Surface of a vector field
ξ	Position in the x-axis of the transformed finite element

η	Position in the y-axis of the transformed finite element
e	The eccentricity, as the distance between the rotor's and stator's centers
c	The difference between R_o and R_i, also called radial clearance
ε	The eccentricity ratio, as the ratio between e and c

CONTENTS

1 INTRODUCTION

Rotating machines are largely applied in industry, such as in compressors, pumps and turbines. A rotating machinery usually consists of disks, shafts, and bearings; all of these elements can be of many shapes, types, and situated at various positions, according to different needs and environments (ISHIDA; YAMAMOTO, 2012). One important application, for example, is in crude oil extraction from under the sea, an important component in Brazilian economy.

When designing such machinery, it is crucial to determine its dynamic behavior, usu-ally referred as rotordynamics, in order to be sure that it will rotate stably, i.e., that its vibration will not exceed safe and acceptable levels, which otherwise could cause excessive wear on bearings or cause seals to fail. Likewise, the understanding of rotordynamics is also important for the diagnosis of a fault when it occurs, as well as for repairing strategies (FRISWELL et al., 2010).

The need for a better understanding of rotordynamics led to the creation of the Rotor-dynamic Open Source Software project (ROSS) [1] (TIMBÓ et al., 2019), an open source library written in Python for rotordynamic analysis. It is stored in the hosting platform GitHub and, as an open source software, it is available for use, change, and distribution.

Among its applications, ROSS allows the construction of a bearing by giving its fluid, and structure parameters. A bearing is the component of a machine composed of a rotating cylinder, called rotor or journal, inside of a slightly larger hollow one, the stator or bearing, with fluid filling the small gap between them. In the case of a horizontal bearing, gravity works and the stator has contact with the rotor when it is still. When the rotor is rotating, a high fluid pressure is created between the rotor and the stator, preventing them to make contact. This high pressure makes the fluid film work equivalently as mass-spring-damper system, causing the rotor to vibrate around an equilibrium position, slightly misplaced from the stator center (ISHIDA; YAMAMOTO, 2012; FRISWELL et al., 2010). Fig 1 shows a simple bearing.

Fig. 2 shows an axial cut of a bearing with its gap exaggerated, and eccentricity e. R_o is the outer radius and R_i is the inner radius as well as the distance between the origin and the gap. Such as in Pina and Carvalho (2006) and Queiroz (2018), differing from Mota et al. (2020) and ROSS, the coordinate system will be attached to the center of the inner cylinder in this work. As well as the center of the coordinate system, the position $\theta = 0$ varies in literature. In this work, θ will begin from the largest gap (dot **A** in Fig. 2)

After instantiating a bearing, ROSS calculates its pressure field using the finite-difference method. With the pressure field, it is possible to calculate the velocity field of

---

[1] <https://github.com/ross-rotordynamics/ross>

Figure 1 – A simple bearing
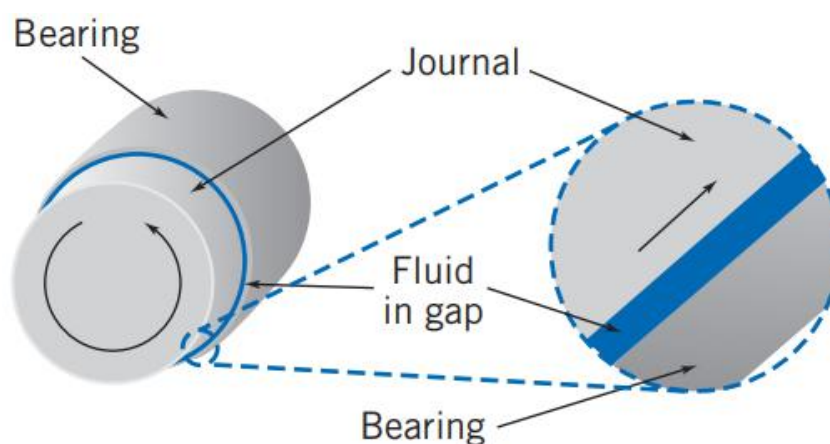
the fluid inside the bearing, as well as the dynamic forces acting on it. The finite-difference method is one among other possibilities of obtaining the pressure field.

1.1 OBJECTIVE

The objective of this work is to compare the use of the finite-element method with the finite-difference method to solve the pressure field inside the bearing, analyzing both approaches. A secondary objective is to implement and make it available a program that provides this solution based on ROSS, in order to allow its future use and integration to the platform. Although the finite-element method is used in other parts of the code, such as in modeling a rotor with disks, shafts, and bearing elements, the bearing pressure field is calculated using the finite-difference method.

1.2 LITERATURE REVIEW

The finite-element method became popular in solving problems in structural mechanics, but it has been largely used for lubrication problems (FRÊNE et al., 1990). One of the advantages of the finite-element method over the finite-difference method is that the first handles irregularly shaped boundaries better, since such boundaries make it difficult to place the grid points using finite difference techniques (BURDEN; FAIRES, 2010). Its weakness, as compared to the finite-difference method, is being more laborious, leading to computer codes of larger size (FRÊNE et al., 1990).

Ishida and Yamamoto (2012) explain the application of finite-element method to rotor systems, stating that it "has been used successfully in the design and analysis of practical rotors with a complicated and irregular shape" (p. 327). Friswell et al. (2010) highlight that, even though the finite-element method is powerful, its derivation is simple and

Figure 2 – Axial cut of a bearing with exaggerated gap
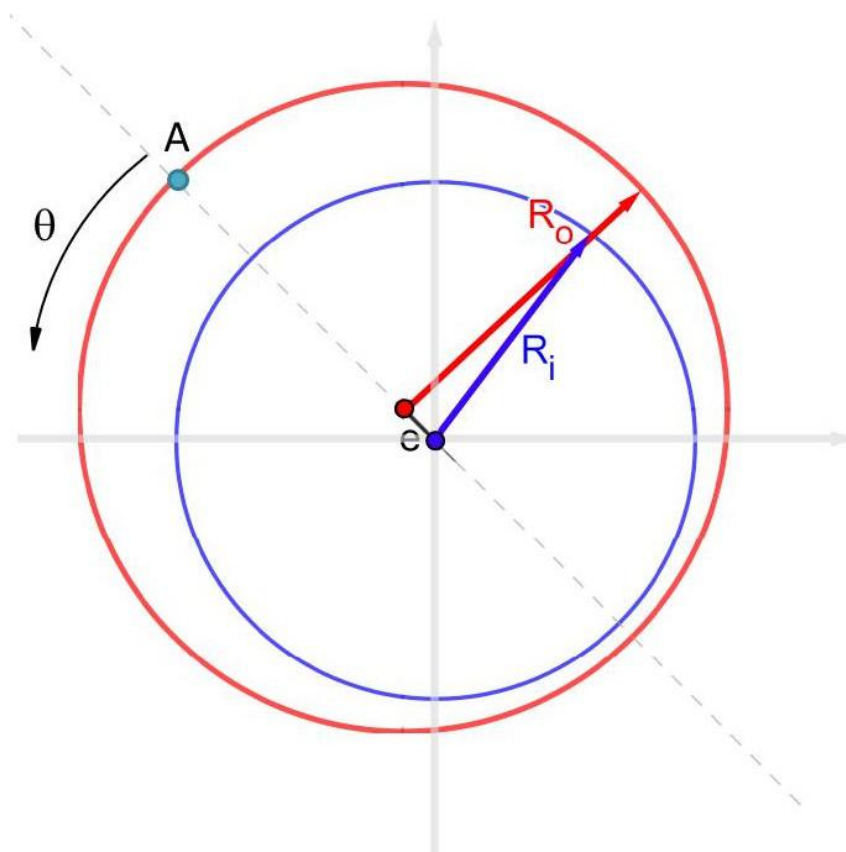
Adapted from: (MOTA; VALÉRIO; RANGEL, 2020)

logical. Because of that, "[it] has developed into a sophisticated method for the analysis of stress, vibration, heat flow, and many other phenomena" (p. 124).

1.3   METHOD

The first step is to introduce the Navier-Stokes equations, that describe the motion of fluids, and obtain their simplification that base the equations used. This allows the fluid pressure to be calculated numerically using a 2-dimensional field. This step is achieved in Chapter 2.

Following the simplification of the Navier-Stokes equations, both finite difference and finite-element methods will be introduced and the later one will be implemented in Python language, using ROSS as one of the packages. The code will be made available online. For that purpose, GitHub will be used as hosting platform and the link will be provided here. Chapter 3 covers the description of both numerical methods.

The numerical analysis is then introduced, detailing the results that will be collected and the tests to be made. These tests will be run for both method, providing graphics are extracted to allow comparison. Chapter 4 introduces the numerical analysis to be

performed and shows the results obtained using both methods.

Finally, the results are discussed in Chapter 5 and a conclusion is presented, as well as future work perspectives.

2 FLUID THEORY

The difference between a fluid and a solid is intuitively known: whereas solids tend to deform or bend, fluids tend to flow when interacted with. A more formal definition, as described by Fox et al. (2011), is that a fluid is a substance that deforms continuously under the application of a tangential stress, no matter how small the stress may be.

Given its properties, a fluid cannot be modeled the same way as a solid object. Its mass is not continuously distributed in space and it will not move altogether and as predictably as a solid would. Instead, fluid properties are treated as continuous above certain volumes, in which the properties are observed to behave predictably. For example, the density of air varies greatly for very small volumes, but becomes stable above 0.001 mm³ at STP (Standard Temperature and Pressure). As a consequence of this continuum assumption, each fluid property is assumed to have a defined value at every point in space above a certain volume and conditions. Likewise, in order to describe its motion, a velocity field is usually applied instead of describing each particle.

2.1 THE NAVIER-STOKES EQUATIONS

Following the continuum assumption, in a system, i.e, a fixed amount of matter, M,

$$M_{system} = \int_{M(system)} dm = \int_{V(system)} \rho dV$$

where dm is a infinitesimal quantity of matter, ρ is the fluid's density (mass per volume), V is the volume and dV is large enough so that we can assume the fluid's properties to be the same for every dV.

In a similar manner, the linear momentum of the system, $\vec{P}$, can be written as

$$\vec{P}_{system} = \int_{M(system)} \vec{v} dm = \int_{V(system)} \vec{v} \rho dV$$

where $\vec{v}$ is the velocity vector in the velocity field, obtained as a function of time, t, and position, $\vec{x}$, which is also a function of time. Therefore, $\vec{v} = \vec{v}(t, \vec{x}(t))$.

In order to compute the acceleration, i.e, the derivative of the velocity, the chain rule must be applied:

$$\frac{D\vec{v}}{Dt} = \frac{\partial \vec{v}}{\partial t} + \frac{\partial \vec{v}}{\partial \vec{x}} \frac{d\vec{x}}{dt}$$

Considering that $\vec{v}$ is a three-dimensional vector, it can be written in terms of its three scalar components. Denoting them in the x, y, and z directions as u, v, and w, respectively, each of them being also a function of time and position, then $\vec{v} = u\hat{i} + v\hat{j} + w\hat{k}$. The

same applies for $\vec{x}$, which can be written in terms of the particle position in coordinates x, y, and z, so $\vec{x}(t) = x_p(t)\hat{i} + y_p(t)\hat{j} + z_p(t)\hat{k}$. Then:

$$\frac{D\vec{v}}{Dt} = \frac{\partial \vec{v}}{\partial t} + \frac{\partial \vec{v}}{\partial x}\frac{dx_p}{dt} + \frac{\partial \vec{v}}{\partial y}\frac{dy_p}{dt} + \frac{\partial \vec{v}}{\partial z}\frac{dz_p}{dt}$$

Since $\dfrac{dx_p}{dt} = u$, $\dfrac{dy_p}{dt} = v$, and $\dfrac{dz_p}{dt} = w$, then:

$$\frac{D\vec{v}}{Dt} = \frac{\partial \vec{v}}{\partial t} + \frac{\partial \vec{v}}{\partial x}u + \frac{\partial \vec{v}}{\partial y}v + \frac{\partial \vec{v}}{\partial z}w$$

Resorting to the gradient operator ∇, the above expression can be simplified as:

$$\frac{D\vec{v}}{Dt} = \frac{\partial \vec{v}}{\partial t} + (\vec{v} \cdot \nabla)\vec{v} \tag{2.1}$$

As for the forces that act on a fluid particle, there are two types: body forces and surface forces, which include normal and tangential (shear) forces (FOX; PRITCHARD; MCDONALD, 2011). Normal stress σ_n and shear stress τ_n acting on the portion of surface δA_n, oriented by the normal vector n, are defined as:

$$\sigma_n = \lim_{\delta A_n \to 0} \frac{\delta F_n}{\delta A_n}$$

$$\tau_n = \lim_{\delta A_n \to 0} \frac{\delta F_n}{\delta A_n}$$

Considering all possible directions of σ_n and τ_n in three mutually perpendicular planes, the stress at any point is specified by nine components. Together they form the Cauchy stress tensor:

$$\sigma = \begin{bmatrix} \sigma_{xx} & \tau_{xy} & \tau_{xz} \\ \tau_{yx} & \sigma_{yy} & \tau_{yz} \\ \tau_{zx} & \tau_{zy} & \sigma_{zz} \end{bmatrix}$$

The stresses can be grouped in the direction that they act to give rise to the surface forces in that direction. Considering as body force dF_B only the force of gravity $\rho\vec{g}$, for each direction the net force dF will be the sum of the force of gravity and the surface force dF_S in that direction. Respectively to x, y, and z:

$$dF_x = dF_{B_x} + dF_{S_x} = \left(\rho g_x + \frac{\partial \sigma_{xx}}{\partial x} + \frac{\partial \tau_{yx}}{\partial y} + \frac{\partial \tau_{zx}}{\partial z}\right)dxdydz$$

$$dF_y = dF_{B_y} + dF_{S_y} = \left(\rho g_y + \frac{\partial \tau_{xy}}{\partial x} + \frac{\partial \sigma_{yy}}{\partial y} + \frac{\partial \tau_{zy}}{\partial z}\right)dxdydz$$

$$dF_z = dF_{B_z} + dF_{S_z} = \left(\rho g_z + \frac{\partial \tau_{xz}}{\partial x} + \frac{\partial \tau_{yz}}{\partial y} + \frac{\partial \sigma_{zz}}{\partial z}\right)dxdydz$$

Considering Newton's second law,

$$d\vec{F} = dm\frac{d\vec{v}}{dt}$$

the differential equations of motion can be obtained by replacing the terms with the expression for the linear momentum (Eq. 2.1) and the above expressions for forces acting on a fluid:

$$d\vec{F} = \rho\left(\frac{\partial\vec{v}}{\partial t} + (\vec{v}\cdot\nabla)\vec{v}\right) \tag{2.2}$$

Assuming a Newtonian fluid of viscosity μ and local pressure p, then the viscous stress is directly proportional to the angular deformation rate - the rate of shearing strain. The stresses may be expressed as follows:

$$\tau_{xy} = \tau_{yx} = \mu\left(\frac{\partial v}{\partial x} + \frac{\partial u}{\partial y}\right)$$

$$\tau_{yz} = \tau_{zy} = \mu\left(\frac{\partial w}{\partial y} + \frac{\partial v}{\partial z}\right)$$

$$\tau_{zx} = \tau_{xz} = \mu\left(\frac{\partial u}{\partial z} + \frac{\partial w}{\partial x}\right)$$

$$\sigma_{xx} = -p - \frac{2}{3}\mu\nabla\cdot\vec{v} + 2\mu\frac{\partial u}{\partial x}$$

$$\sigma_{yy} = -p - \frac{2}{3}\mu\nabla\cdot\vec{v} + 2\mu\frac{\partial v}{\partial y}$$

$$\sigma_{zz} = -p - \frac{2}{3}\mu\nabla\cdot\vec{v} + 2\mu\frac{\partial w}{\partial z}$$

If these expressions are introduced into the differential equations of motion (Eq. 2.2), the resulting equations of motion are called Navier-Stokes equations. Such equations are greatly simplified when applied to incompressible flow with constant viscosity, in which case they are reduced to (FOX; PRITCHARD; MCDONALD, 2011):

$$\rho\left(\frac{\partial\vec{v}}{\partial t} + \vec{v}\cdot\nabla\vec{v}\right) = \rho\vec{g} - \nabla p + \mu\nabla^2\vec{v}$$

2.2 FURTHER SIMPLIFYING THE NAVIER-STOKES EQUATIONS

The following manipulations of the Navier-Stokes equations, as well as the ones in next section, have been extensively showed and applied in the fluid field involving flow in the annular space between two cylinders. A few previous works of the kind include the one by Queiroz (2018), by de Pina and Carvalho (2006), and by Andrade (2008). Still, the manipulations were kept here for educational purposes.

In this work, the system is assumed to have reached a steady state, after accelerating for a while, meaning that, for the properties of the system, the partial derivative with respect to time is equal to zero and remains so: $\dfrac{\partial(*)}{\partial t} = 0$. Thus, $\dfrac{\partial \vec{v}}{\partial t} = 0$ and the Navier-Stokes equation can be rewritten as:

$$\rho(\vec{v} \cdot \nabla \vec{v}) = \rho \vec{g} - \nabla p + \mu \nabla^2 \vec{v}$$

For the purpose of simplifying the equation, no body forces will be considered, which means the gravity force will be neglected. Then:

$$\rho(\vec{v} \cdot \nabla \vec{v}) = -\nabla p + \mu \nabla^2 \vec{v}$$

As the journal bearing system is a cylindrical one, it is possible to use a cylindrical coordinates system and take advantage of the geometry by doing so. Rewriting the Navier-Stokes equations in cylindrical coordinates, assuming that u, v, and w are now the velocities in the axial-axis (z-axis), radial-axis (r-axis), and tangential-axis (θ-axis), respectively, results in:

- on the z-axis:

$$
\begin{aligned}
&\rho\left(u\frac{\partial u}{\partial z} + v\frac{\partial u}{\partial r} + \frac{w}{r}\frac{\partial u}{\partial \theta}\right) = \\
&-\frac{\partial p}{\partial z} + \mu\left(\frac{1}{r}\frac{\partial}{\partial r}\left[r\frac{\partial u}{\partial r}\right] + \frac{1}{r^2}\frac{\partial^2 u}{\partial \theta^2} + \frac{\partial^2 u}{\partial z^2}\right)
\end{aligned}
\tag{2.3}
$$

- on the r-axis:

$$
\begin{aligned}
&\rho\left(u\frac{\partial v}{\partial z} + v\frac{\partial v}{\partial r} + \frac{w}{r}\frac{\partial v}{\partial \theta} - \frac{w^2}{r}\right) = \\
&-\frac{\partial p}{\partial r} + \mu\left(\frac{\partial}{\partial r}\left[\frac{1}{r}\frac{\partial(rv)}{\partial r}\right] + \frac{1}{r^2}\frac{\partial^2 v}{\partial \theta^2} - \frac{2}{r^2}\frac{\partial w}{\partial \theta} + \frac{\partial^2 v}{\partial z^2}\right)
\end{aligned}
\tag{2.4}
$$

- on the θ-axis:

$$
\begin{aligned}
&\rho\left(u\frac{\partial w}{\partial z} + v\frac{\partial w}{\partial r} + \frac{w}{r}\frac{\partial w}{\partial \theta} + \frac{vw}{r}\right) = \\
&-\frac{1}{r}\frac{\partial p}{\partial \theta} + \mu\left(\frac{\partial}{\partial r}\left[\frac{1}{r}\frac{\partial(rw)}{\partial r}\right] + \frac{1}{r^2}\frac{\partial^2 w}{\partial \theta^2} + \frac{2}{r^2}\frac{\partial v}{\partial \theta} + \frac{\partial^2 w}{\partial z^2}\right)
\end{aligned}
\tag{2.5}
$$

By performing a dimensional analysis, a technique for gaining insight into many engineering and scientific phenomena (FOX; PRITCHARD; MCDONALD, 2011), the following equalities are considered, introducing a few dimensionless variables represented by a

'^' above them: $u = \hat{u}U$, $v = \hat{v}U$, $w = \hat{w}U$, $p = \hat{p}P$, $z = \hat{z}L$, $r = \hat{r}F$, $r\theta = \hat{r}\theta L$; being U a typical velocity, P a typical pressure, L a typical length, $F = R_o - R_i$, with L, R_o, and R_i of the same order of magnitude. Notice that $F \ll L$. Replacing these variables in Eq. 2.3, and rearranging it, using the fact that $P = \dfrac{\mu U L}{F^2}$, results in:

$$\left(\frac{\rho U^2}{L}\right)\left(\hat{u}\frac{\partial \hat{u}}{\partial \hat{z}} + \left(\frac{L}{F}\right)\hat{v}\frac{\partial \hat{u}}{\partial \hat{r}} + \frac{\hat{w}}{\hat{r}}\frac{\partial \hat{u}}{\partial \theta}\right) =$$
$$\left(\frac{\mu U}{F^2}\right)\left(-\frac{\partial \hat{p}}{\partial \hat{z}} + \mu\left(\frac{1}{\hat{r}}\frac{\partial}{\partial \hat{r}}\left[\hat{r}\frac{\partial \hat{u}}{\partial \hat{r}}\right] + \left(\frac{F^2}{L^2}\right)\frac{1}{\hat{r}^2}\frac{\partial^2 \hat{u}}{\partial \theta^2} + \left(\frac{F^2}{L^2}\right)\frac{\partial^2 \hat{u}}{\partial \hat{z}^2}\right)\right) \tag{2.6}$$

By multiplying both sides of above equation by $\dfrac{L^2}{\mu U}$, the Reynolds number appears on the right side:

$$\left(\frac{\rho U L}{\mu}\right)\left(\hat{u}\frac{\partial \hat{u}}{\partial \hat{z}} + \left(\frac{L}{F}\right)\hat{v}\frac{\partial \hat{u}}{\partial \hat{r}} + \frac{\hat{w}}{\hat{r}}\frac{\partial \hat{u}}{\partial \theta}\right) =$$
$$\left(\frac{L^2}{F^2}\right)\left(-\frac{\partial \hat{p}}{\partial \hat{z}} + \mu\left(\frac{1}{\hat{r}}\frac{\partial}{\partial \hat{r}}\left[\hat{r}\frac{\partial \hat{u}}{\partial \hat{r}}\right] + \left(\frac{F^2}{L^2}\right)\frac{1}{\hat{r}^2}\frac{\partial^2 \hat{u}}{\partial \theta^2} + \left(\frac{F^2}{L^2}\right)\frac{\partial^2 \hat{u}}{\partial \hat{z}^2}\right)\right) \tag{2.7}$$

The Reynolds number, a dimensionless measure, usually denoted as Re, predicts with a high degree of accuracy whether the flow is laminar (in case of a small Re) or turbulent (in case of a large Re) (FOX; PRITCHARD; MCDONALD, 2011).

Multiplying both sides of Eq. 2.7 by $\dfrac{F^2}{L^2}$ and using $Re = \dfrac{\rho U L}{\mu}$ results in:

$$Re\left(\left(\frac{F^2}{L^2}\right)\hat{u}\frac{\partial \hat{u}}{\partial \hat{z}} + \left(\frac{F}{L}\right)\hat{v}\frac{\partial \hat{u}}{\partial \hat{r}} + \left(\frac{F^2}{L^2}\right)\frac{\hat{w}}{\hat{r}}\frac{\partial \hat{u}}{\partial \theta}\right) =$$
$$-\frac{\partial \hat{p}}{\partial \hat{z}} + \mu\left(\frac{1}{\hat{r}}\frac{\partial}{\partial \hat{r}}\left[\hat{r}\frac{\partial \hat{u}}{\partial \hat{r}}\right] + \left(\frac{F^2}{L^2}\right)\frac{1}{\hat{r}^2}\frac{\partial^2 \hat{u}}{\partial \theta^2} + \left(\frac{F^2}{L^2}\right)\frac{\partial^2 \hat{u}}{\partial \hat{z}^2}\right) \tag{2.8}$$

Since $F \ll L$, terms multiplying $\dfrac{F}{L}$ or $\dfrac{F^2}{L^2}$ may be neglected. Therefore, the motion equation on z-axis becomes (after returning dimensions to dimensionless terms):

$$-\frac{\partial p}{\partial z} + \mu\left[\frac{1}{r}\frac{\partial}{\partial r}\left(r\frac{\partial u}{\partial r}\right)\right] = 0 \tag{2.9}$$

By applying the dimensional analysis into Eqs. 2.4 and 2.5, r-axis and θ-axis become, respectively:

$$-\frac{\partial p}{\partial r} = 0 \tag{2.10}$$

$$-\frac{1}{r}\frac{\partial p}{\partial \theta} + \mu\left[\frac{\partial}{\partial r}\left(\frac{1}{r}\frac{\partial(rw)}{\partial r}\right)\right] = 0 \tag{2.11}$$

Based on Eq. 2.10, it is possible to conclude that the pressure is constant along the r-axis. Also, v, the radial velocity, is no longer present in the system, thus it is not significant in comparison with u and w.

2.3   SOLVING THE SIMPLIFIED NAVIER-STOKES EQUATIONS

Now we can integrate both Eqs. 2.9 and 2.11 in order to isolate u and w, obtaining velocities on z-axis and *theta*-axis. Beginning with Eq. 2.9, by rearranging and integrating twice in r we obtain:

$$u = \frac{\partial p}{\partial z}\frac{r^2}{4} + c_1 \ln r + c_2 \tag{2.12}$$

Experiments with laminar pipe flows show that the velocity at the wall is zero along the entire length of the pipe (FOX; PRITCHARD; MCDONALD, 2011), therefore the two boundary conditions necessary to determine a unique solution to Eq. 2.12 can be defined simply as:

$$u(R_o) = 0$$

$$u(R_i) = 0$$

By applying these conditions into Eq. 2.12, we get to determine c_1 and c_2 as:

$$c_2 = -\frac{\partial p}{\partial z}\frac{R_i^2}{4} - c_1 \ln R_i$$

$$c_1 = \frac{\frac{1}{4}\frac{\partial p}{\partial z}(R_i^2 - R_o^2)}{\ln \frac{R_o}{R_i}}$$

Finally, by replacing c_1 and c_2 in 2.12, we get to:

$$u = \frac{1}{4}\frac{\partial p}{\partial z}R_i^2 \left[\left(\frac{r}{R_i}\right)^2 - \frac{(R_o^2 - R_i^2)}{R_i^2 \ln \frac{R_o}{R_i}}\left(\ln \frac{r}{R_i}\right) - 1 \right] \tag{2.13}$$

Now we turn to Eq 2.11 in order to find a suitable expression for w. By rearranging it and integrating it twice in r we get to:

$$w = \frac{1}{2}\frac{\partial p}{\partial \theta}r\left(\ln r - \frac{1}{2}\right) + c_3 r + \frac{c_4}{r} \tag{2.14}$$

Same as in Eq. 2.12, we require two boundary conditions for a unique solution. Since we want the velocity along the θ-axis, and the stator is still while the rotor is spinning at an angular velocity ω, w at R_o must be zero whereas w at R_i must be ωR_i, i.e., W. Thus:

$$w(R_o) = 0$$

$$w(R_i) = \omega R_i = W$$

Then:

$$c_4 = -\frac{1}{2}\frac{\partial p}{\partial \theta}R_o^2\left(\ln R_o - \frac{1}{2}\right) - c_3 R_o^2$$

$$c_3 = \frac{\frac{1}{2}\frac{\partial p}{\partial \theta}}{(R_i^2 - R_o^2)}\left[R_o^2\left(\ln R_o - \frac{1}{2}\right) - R_i^2\left(\ln R_i - \frac{1}{2}\right)\right] + \frac{WR_i}{(R_i^2 - R_o^2)}$$

Finally, by replacing c_3 and c_4 in 2.14, we get to:

$$w = \frac{1}{2}\frac{\partial p}{\partial \theta}\left[r\left(\ln r - \frac{1}{2}\right) + Kr - \frac{R_o^2}{r}\left(\ln R_o + K - \frac{1}{2}\right)\right] + \frac{WR_i}{(R_i^2 - R_o^2)}\left(r - \frac{R_o^2}{r}\right) \quad (2.15)$$

in which

$$K = \frac{1}{(R_i^2 - R_o^2)}\left[R_o^2\left(\ln R_o - \frac{1}{2}\right) - R_i^2\left(\ln R_i - \frac{1}{2}\right)\right]$$

Notice that, so far, we have been dealing with four unknowns - namely, u, v, w, and p) - and no more than three equations: Eqs. 2.9, 2.10, 2.11, and their products. Even if we take out Eq. 2.10, we are left with three unknowns and two equations. We now require one more equation in order to build a linear system with the possibility of a unique solution, therefore we introduce the continuity equation, that describes the mass conservation of a system:

$$\frac{\partial \rho}{\partial t} + \nabla \cdot (\rho \vec{v}) = 0$$

But since the system is in steady state ($\frac{\partial(*)}{\partial t} = 0$) and ρ is constant, the continuity equation is reduced to:

$$\nabla \cdot \vec{v} = 0$$

In cylindrical coordinates, it is written as:

$$\frac{1}{r}\frac{\partial(rv)}{\partial r} + \frac{1}{r}\frac{\partial w}{\partial \theta} + \frac{\partial u}{\partial z} = 0$$

By rearranging and integrating it, we get to:

$$\int_{R_i}^{R_o}\left(\frac{\partial(rv)}{\partial r} + \frac{\partial w}{\partial \theta} + \frac{\partial(ru)}{\partial z}\right)dr = 0 \quad (2.16)$$

By applying the distributive property, we may write above equation as the sum of three integrals and solve each one separately. For the first one, we can use the fundamental

theorem of calculus, whereas the second and third can be solved by using Leibniz integral rule:

- I) $\int_{R_i}^{R_o} \frac{\partial (rv)}{\partial r}\,\mathrm{d}r = R_o v(R_o) - R_i v(R_i)$

- II) $\int_{R_i}^{R_o} \frac{\partial w}{\partial \theta}\,\mathrm{d}r = \frac{\partial}{\partial \theta}\int_{R_i}^{R_o} w\,\mathrm{d}r - \left[w(R_o)\frac{\partial R_o}{\partial \theta} - w(R_i)\frac{\partial R_i}{\partial \theta}\right]$

- III) $\int_{R_i}^{R_o} \frac{\partial (ru)}{\partial z}\,\mathrm{d}r = \frac{\partial}{\partial z}\int_{R_i}^{R_o} ru\,\mathrm{d}r - \left[R_o u(R_o)\frac{\partial R_o}{\partial z} - R_i u(R_i)\frac{\partial R_i}{\partial z}\right]$

A few considerations can be made regarding above expressions: v is negligible, so (I) is not significant; in (II), $\frac{\partial R_i}{\partial \theta} = 0$ and $w(R_o) = 0$; in (III), $u(R_o) = u(R_i) = 0$. Rewriting Eq. 2.16 with these considerations results in:

$$\frac{\partial}{\partial \theta}\int_R w\,\mathrm{d}r + \frac{\partial}{\partial z}\int_R ru\,\mathrm{d}r = 0$$

If we use u and w from Eqs. 2.13 and 2.15 and then calculate the integrals, the result is

$$\frac{\partial}{\partial \theta}\left(\alpha \frac{\partial p}{\partial \theta}\right) + \frac{\partial}{\partial z}\left(\beta \frac{\partial p}{\partial z}\right) = \frac{\partial}{\partial \theta}\gamma \tag{2.17}$$

where

$$\gamma = -WR_i\left[\ln\left(\frac{R_o}{R_i}\right)\left(1 + \frac{R_i^2}{(R_o^2 - R_i^2)}\right) - \frac{1}{2}\right] \tag{2.18}$$

$$\alpha = \frac{1}{4}\left[R_o^2 \ln R_o - R_i^2 \ln R_i + (R_o^2 - R_i^2)(K-1)\right] - \left[\left(\ln R_o + K - \frac{1}{2}\right)\ln\left(\frac{R_o}{R_i}\right)\right] \tag{2.19}$$

$$\beta = \frac{-R_i^2}{8}\left\{\left[R_o^2 - R_i^2 - \frac{(R_o^4 - R_i^4)}{2R_i^2}\right] + \left(\frac{R_o^2 - R_i^2}{R_i^2 \ln(R_o/R_i)}\right)\left[R_o^2 \ln\left(\frac{R_o}{R_i}\right) - \frac{(R_o^2 - R_i^2)}{2}\right]\right\} \tag{2.20}$$

Eq. 2.17 is of type $\frac{\partial^2 u}{\partial x^2}(x,y) + \frac{\partial^2 u}{\partial y^2}(x,y) = f(x,y)$, which is known as the Poisson equation (BURDEN; FAIRES, 2010). Such equation cannot be solved analytically, therefore we must resort to numerical methods in order to find its solution. In our case, solving Eq. 2.17 will give the pressure in each position of the fluid.

3 NUMERICAL METHODS FOR SOLVING POISSON EQUATION

3.1 THE FINITE-DIFFERENCE METHOD

Additional constraints must be imposed to obtain a unique solution of the Poisson equation. This is usually given by the boundary region of the plane described by the equation, then a numerical method can be applied, such as the finite-difference method. It consists in replacing each of the derivatives in the differential equation with an appropriated difference-quotient approximation, then dividing the interval into equal subintervals, choosing a step size that is small enough to get a close approximation of the derivatives, but not too small because of the general instability of the derivative approximations (BURDEN; FAIRES, 2010). This strategy creates a grid over the plane represented by the equation, as in Fig. 3, where the intersection of lines are the mesh points of the grid (θ_i, z_j), for $i = 0, 1, ..., N_\theta$ and $j = 0, 1, ..., N_Z$, where N_θ and N_Z are the number of mesh points in azimuthal direction and axial direction, respectively. Whereas z_j ranges from 0 to the length of the bearing, which we call L, θ_i ranges from 0 to 2π, to represent the bearing's circumference.

Figure 3 – Grid over the plane
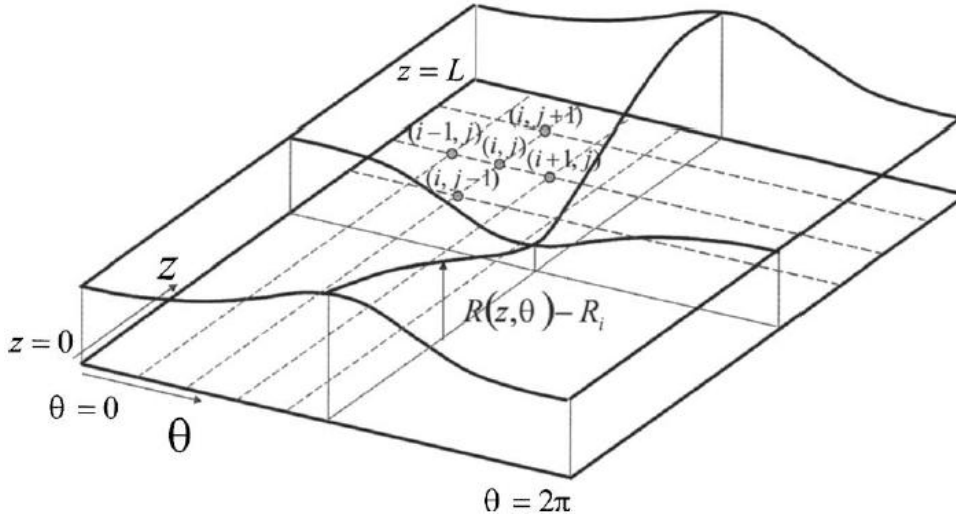
Source: (PINA; CARVALHO, 2006, p. 4)

In our case, the boundary region along both sides of the bearing is defined as

$$p(\theta_i, z = 0) = P_{in}$$

$$p(\theta_i, z = L) = P_{out}$$

where P_{in} and P_{out} are the pressure values at both sides of the bearing. Notice that there is no actual boundary at $(\theta_i = 0, z_j)$ and $(\theta_i = 2\pi, z_j)$, but still these points are constrained by the fact that they must present the same value when in the same line z_j. That is:

$$p(\theta = 0, z_j) = p(\theta = 2\pi, z_j)$$

The mesh points that do not belong to the boundary region, where the values are known, can have their pressure value calculated based on previous and next values with the applied discretization:

$$\frac{\partial}{\partial \theta}\left(\alpha\frac{\partial p}{\partial \theta}\right) = \frac{1}{\Delta\theta}\left[\alpha_{i,j}\left(\frac{p_{i+1,j} - p_{i,j}}{\Delta\theta}\right) - \alpha_{i-1,j}\left(\frac{p_{i,j} - p_{i-1,j}}{\Delta\theta}\right)\right]$$

$$\frac{\partial}{\partial z}\left(\beta\frac{\partial p}{\partial z}\right) = \frac{1}{\Delta z}\left[\beta_{i,j}\left(\frac{p_{i,j+1} - p_{i,j}}{\Delta z}\right) - \beta_{i,j-1}\left(\frac{p_{i,j} - p_{i,j-1}}{\Delta z}\right)\right]$$

$$\frac{\partial}{\partial \theta}\gamma = \frac{1}{\Delta\theta}\left[\gamma_{i,j} - \gamma_{i-1,j}\right]$$

This discretization allows us to build a linear system with the same number of equations and unknowns, i.e., of unique solution. The unknowns are p in every mesh point of the grid. The result is a pressure matrix that can be used to calculate $\vec{v}$ in every mesh point by resorting to Eqs. 2.13 and 2.15.

3.2   THE FINITE-ELEMENT METHOD

Along with the finite-difference method, another possibility is the finite-element method. The main difference between the two of them is that the finite-element method allows irregular shaping of the boundary and even of the grid itself. Considering Eq. 2.17, our main differential equation, the method seeks an approximation of the function p of the form

$$\phi(\theta, z) = \sum_{i=1}^{N_T} C_i\varphi_i(\theta, z)$$

where N_T is the total number of nodes in the grid, C_1, C_2, ..., C_{N_T} are constants, and φ_1, φ_2, ..., φ_{N_T} are called basis functions. These functions are equal to one on the one node numbered with the same number as them and are equal to zero on every other node.

Instead of solving Eq. 2.17, referred as the strong form (RINCON; LIU, 2015), the finite-element method solves the weak form, which is given by the integral of the residual multiplied by a weighting function, over the entire region. In our case, it is given by

$$\int_{\Omega} \kappa\left[\frac{\partial}{\partial \theta}\left(\alpha\frac{\partial p}{\partial \theta}\right) + \frac{\partial}{\partial z}\left(\beta\frac{\partial p}{\partial z}\right) - \frac{\partial}{\partial \theta}\gamma\right]d\Omega = 0 \tag{3.1}$$

where Ω refers to the region of the θ-z-plane and κ is a weighting function. The idea is to satisfy the differential equation in an average sense, approximating the solution by minimizing the integral over a smaller set of functions, not over all points of p. Considering Eq. 2.17 and its boundary conditions, both its strong and weak forms are equivalent, as it possible to go to Eq. 3.1 from 2.17 and back; therefore solving the weak form is equivalent to solving the strong form.

In order to reduce the number of derivatives of p, that way demanding only that its first derivative is smooth, a few steps can be taken. First, using the relation that comes from the derivative of the product of two functions:

$$\frac{d}{d\theta}\left[\kappa\left(\alpha\frac{dp}{d\theta}\right)\right] = \frac{d\kappa}{d\theta}\left(\alpha\frac{dp}{d\theta}\right) + \kappa\frac{d}{d\theta}\left(\alpha\frac{dp}{d\theta}\right)$$

Rearranging it:

$$\kappa\frac{d}{d\theta}\left(\alpha\frac{dp}{d\theta}\right) = -\frac{d\kappa}{d\theta}\left(\alpha\frac{dp}{d\theta}\right) + \frac{d}{d\theta}\left[\kappa\left(\alpha\frac{dp}{d\theta}\right)\right]$$

Then using the distributive property of the integral, it is possible to modify the first term of Eq. 3.1:

$$\int_\Omega \kappa\frac{\partial}{\partial\theta}\left(\alpha\frac{\partial p}{\partial\theta}\right)d\Omega = -\int_\Omega \frac{\partial\kappa}{\partial\theta}\left(\alpha\frac{\partial p}{\partial\theta}\right)d\Omega + \int_\Omega \frac{\partial}{\partial\theta}\left[\kappa\left(\alpha\frac{\partial p}{\partial\theta}\right)\right]d\Omega$$

By applying the same steps to the second term of Eq. 3.1 and rearranging it, we get to:

$$\int_\Omega \left[-\alpha\frac{\partial\kappa}{\partial\theta}\frac{\partial p}{\partial\theta} - \beta\frac{\partial\kappa}{\partial z}\frac{\partial p}{\partial z}\right]d\Omega = \int_\Omega \kappa\frac{\partial}{\partial z}\gamma d\Omega - \int_\Omega \left[\frac{\partial}{\partial\theta}\left(\kappa\alpha\frac{\partial p}{\partial\theta}\right) + \frac{\partial}{\partial z}\left(\kappa\beta\frac{\partial p}{\partial z}\right)\right]d\Omega$$

Finally, we resort to the divergence theorem, which states that the volume integral of the divergence of a vector field over the region inside a closed surface is equal to the surface integral of a vector field over the surface. This theorem can be mathematically represented by

$$\int_\Omega \nabla \cdot \boldsymbol{f} d\Omega = \int_\Gamma \boldsymbol{n} \cdot \boldsymbol{f} d\Gamma$$

where $\boldsymbol{f}$ is the vector field, Γ is its surface and $\boldsymbol{n}$ is the normal vector in each point of the surface. In our case, the vector field is given by $\begin{bmatrix} \kappa\alpha\frac{\partial p}{\partial\theta} \\ \kappa\beta\frac{\partial p}{\partial z} \end{bmatrix}$, but because κ is chosen in a way that it is equal to zero over the boundary, the result of the integral on the right side of above equation is equal to zero. Therefore:

$$\int_\Omega \left[-\alpha\frac{\partial\kappa}{\partial\theta}\frac{\partial p}{\partial\theta} - \beta\frac{\partial\kappa}{\partial z}\frac{\partial p}{\partial z}\right]d\Omega = \int_\Omega \kappa\frac{\partial}{\partial z}\gamma d\Omega \tag{3.2}$$

As the function ϕ is zero along unknown nodes of the grid, we must still define an approximation of p to replace in Eq. 3.2. We will define this function as $p_a \approx p$:

$$p_a(\theta, z) = \phi(\theta, z) + q(\theta, z)$$

where q is a function that satisfies the same boundary conditions of p, but is zero over unknown nodes:

$$q(\theta, z) = \begin{cases} P_{in} & , z = 0 \\ P_{out} & , z = L \\ 0 & , z \neq 0, L \end{cases}$$

The function q can be represented the same way as ϕ, as a sum of constants q_i multiplied by φ_i. However, in this case we know the values of q_i. The same applies to the right side of equation 2.17, which we will call function f and f_i its constants. Therefore:

$$q(\theta, z) = \sum_{i=1}^{N_T} q_i \varphi_i(\theta, z)$$

$$f(\theta, z) = \sum_{i=1}^{N_T} f_i \varphi_i(\theta, z) = \varphi_i(\theta, z) \frac{\partial}{\partial z} \gamma(\theta, z)$$

We then replace p with p_a in Eq. 3.2. We will also define the weighting function as the function φ_i, that way maintaining its restriction of being equal to zero over the boundary. Using the distributive property of both integral and derivative, we can rearrange the equation such as:

$$\int_\Omega \left[-\alpha \frac{\partial \varphi_i}{\partial \theta} \frac{\partial \phi}{\partial \theta} - \beta \frac{\partial \varphi_i}{\partial z} \frac{\partial \phi}{\partial z} \right] d\Omega = \int_\Omega \varphi_i \frac{\partial}{\partial z} \gamma d\Omega + \int_\Omega \left[\alpha \frac{\partial \varphi_i}{\partial \theta} \frac{\partial q}{\partial \theta} + \beta \frac{\partial \varphi_i}{\partial z} \frac{\partial q}{\partial z} \right] d\Omega$$

Because ϕ and q are sums of constants, these constants can be pulled out of the integral and the derivative. We will also use the function f defined above and pull its constants out of the integral. Therefore:

$$\sum_{j=1}^{N_T} C_j \int_\Omega \left[-\alpha \frac{\partial \varphi_i}{\partial \theta} \frac{\partial \varphi_j}{\partial \theta} - \beta \frac{\partial \varphi_i}{\partial z} \frac{\partial \varphi_j}{\partial z} \right] d\Omega =$$

$$\sum_{j=1}^{N_T} f_j \int_\Omega \varphi_i \varphi_j d\Omega + \sum_{j=1}^{N_T} q_j \int_\Omega \left[\alpha \frac{\partial \varphi_i}{\partial \theta} \frac{\partial \varphi_j}{\partial \theta} + \beta \frac{\partial \varphi_i}{\partial z} \frac{\partial \varphi_j}{\partial z} \right] d\Omega \tag{3.3}$$

Now we define:

$$K_{ij} = \int_\Omega \left[-\alpha \frac{\partial \varphi_i}{\partial \theta} \frac{\partial \varphi_j}{\partial \theta} - \beta \frac{\partial \varphi_i}{\partial z} \frac{\partial \varphi_j}{\partial z} \right] d\Omega$$

$$F_i = \sum_{j=1}^{N_T} f_j \int_\Omega \varphi_i \varphi_j d\Omega + \sum_{j=1}^{N_T} q_j \int_\Omega \left[\alpha \frac{\partial \varphi_i}{\partial \theta} \frac{\partial \varphi_j}{\partial \theta} + \beta \frac{\partial \varphi_i}{\partial z} \frac{\partial \varphi_j}{\partial z} \right] d\Omega$$

Finally, the problem can be rewritten in its matrix form:

$$KC = F$$

3.3 AN EXAMPLE OF FINITE-ELEMENT METHOD

The region Ω is divided in small regions Ω_e: the finite elements. Regardless of how this is done, each node is uniquely numbered and two Tables are kept for the purpose of identification: one containing the nodes in each element and another one containing the position of the node's equation in the linear system. Let us take this example by Rincon and Liu to better understand how this is done. Consider the region in Fig. 4 and Tables 1 and 2.

Figure 4 – Region divided in 16 finite elements

Source: (RINCON; LIU, 2015, p. 111)

Table 1 – Nodes per element

$a\backslash e$	1	2	3	4	5	6	7	8	9	10	11	12	13	14	15	16
1	1	2	3	4	6	7	8	9	11	12	13	14	16	17	18	19
2	2	3	4	5	7	8	9	10	12	13	14	15	17	18	19	20
3	7	8	9	10	12	13	14	15	17	18	19	20	22	23	24	25
4	6	7	8	9	11	12	13	14	16	17	18	19	21	22	23	24

Source: (RINCON; LIU, 2015, p. 139)

Table 2 – Equation per node

A	1	2	3	4	5	6	7	8	9	10	11	12	13
$\text{eqn}[A]$	0	1	0	2	0	3	4	5	6	7	8	9	10
A	14	15	16	17	18	19	20	21	22	23	24	25	
$\text{eqn}[A]$	11	12	13	14	15	16	17	18	0	19	0	20	

Source: (RINCON; LIU, 2015, p. 139)

Together, Tables 1 and 2 represent the region in Fig. 4, divided in 16 elements, 4 elements per axis, with 4 nodes each. Table 1 identifies the 4 local nodes a in each element, numbered locally from 1 to 4, counterclockwise, beginning with the lowest (x, y), whereas Table 2 contains the row in the linear system for the equation (eqn) involving each node A. Nodes in which the value is known are marked with zero in Table 2, as they have no place in the linear system. In this example, such nodes are the nodes 1, 3, 5, 22, and 24. These Tables gather enough information to implement routines that map how the region is divided and mount the global matrices based on local parameters.

3.4 CALCULATING THE GLOBAL MATRICES

The region Ω_e of an element e consists of a $[x_i,\ x_{i+1}]$ x $[y_j,\ y_{j+1}]$ rectangle. Or, in another representation, $[x_1^e,\ x_2^e]$ x $[y_1^e,\ y_2^e]$. This way, considering the finite element in Fig. 5, with nodes locally numbered from 1 to 4. These are the φ_i^e functions that apply to it, also represented in Fig. 5:
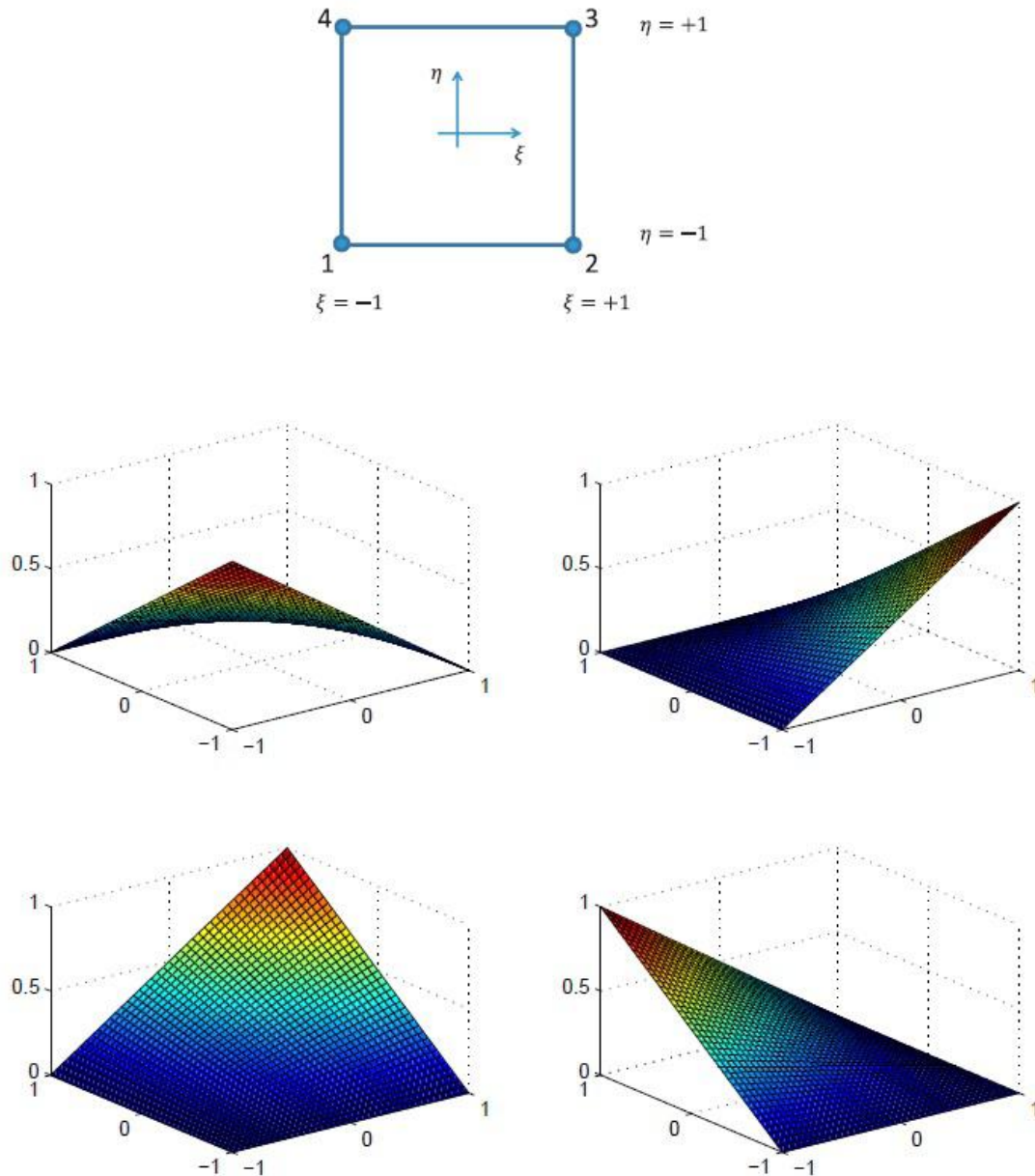
$$\varphi_2^e(x,y) = \frac{(x - x_2^e)(y - y_2^e)}{(x_1^e - x_2^e)(y_1^e - y_2^e)}$$

$$\varphi_2^e(x,y) = \frac{(x - x_1^e)(y - y_2^e)}{(x_2^e - x_1^e)(y_1^e - y_2^e)}$$

$$\varphi_3^e(x,y) = \frac{(x - x_1^e)(y - y_1^e)}{(x_2^e - x_1^e)(y_2^e - y_1^e)}$$

$$\varphi_4^e(x, y) = \frac{(x - x_2^e)(y - y_1^e)}{(x_1^e - x_2^e)(y_2^e - y_1^e)}$$

Figure 5 – One finite element of 4 nodes and its base functions

Source: (CARVALHO; VALÉRIO, 2012, p. 68)

They are called φ_i^e functions because they only apply to the region Ω_e of the element e, and to distinguish from the φ_i functions that apply to Ω. They can be related to their correspondent φ_i functions using Table 1.

The contribution of a rectangular finite element with 4 nodes to the global matrices is calculated locally over Ω_e. The values from Ω_e are then added to the local matrices K^e and F^e. The global matrices K and F will be a result of the sum of the local matrices of all elements. Each position in K^e and F^e are obtained as:
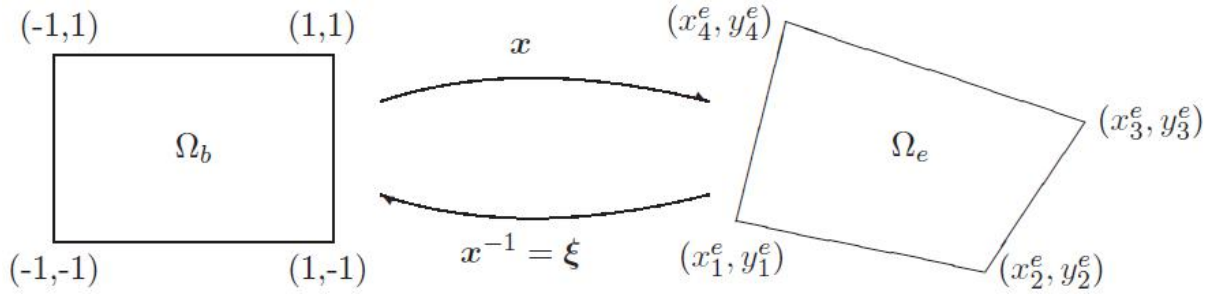
$$K_{ab}^e = \int_{\Omega_e} \left[-\alpha \frac{\partial \varphi_a}{\partial \xi} \frac{\partial \varphi_b}{\partial \xi} - \beta \frac{\partial \varphi_a}{\partial \eta} \frac{\partial \varphi_b}{\partial \eta} \right] d\Omega_e$$

$$F_a^e = \sum_{b=1}^{4} f_b^e \int_{\Omega_e} \varphi_a \varphi_b d\Omega_e + \sum_{b=1}^{4} q_b \int_{\Omega_e} \left[\alpha \frac{\partial \varphi_a}{\partial \xi} \frac{\partial \varphi_b}{\partial \xi} + \beta \frac{\partial \varphi_a}{\partial \eta} \frac{\partial \varphi_b}{\partial \eta} \right] d\Omega_e$$

Notice that K^e is a 4 x 4 matrix and F^e is a 4 x 1 one.

K^e and F^e are not obtained directly though. They are calculated over a [-1, 1] x [-1, 1] square, represented as region Ω_b, and then transformed to the real values using a transformation matrix, through a isoparametric mapping, as in Fig. 6,

Figure 6 – One finite element of 4 nodes

Source: (RINCON; LIU, 2015, p. 123)

in which $\boldsymbol{x} = \boldsymbol{x}(\boldsymbol{\xi}) = (\theta, z)$ and $\boldsymbol{\xi} = \boldsymbol{\xi}(\boldsymbol{x}) = (\xi, \eta)$.

Since nodes 1, 2, 3, and 4 are located in positions $(-1, -1)$, $(1, -1)$, $(1, 1)$, and $(-1, 1)$, respectively, in the region Ω_b, the φ_i functions get a simple solution:

$$\varphi_1(\xi, \eta) = \frac{1}{4}(1 - \xi)(1 - \eta)$$

$$\varphi_2(\xi, \eta) = \frac{1}{4}(1 + \xi)(1 - \eta)$$

$$\varphi_3(\xi, \eta) = \frac{1}{4}(1 + \xi)(1 + \eta)$$

$$\varphi_4(\xi, \eta) = \frac{1}{4}(1 - \xi)(1 + \eta)$$

This isoparametric mapping is defined by:

$$\begin{cases} \theta(\xi, \eta) = \sum_{i=1}^{4} \theta_i \varphi_i(\xi, \eta) \\ z(\xi, \eta) = \sum_{i=1}^{4} z_i \varphi_i(\xi, \eta) \end{cases}$$

Now, in possession of this coordinate mapping, it is possible to determine:

$$\begin{cases} \dfrac{\partial \varphi_i}{\partial \xi} = \dfrac{\partial \varphi_i}{\partial \theta}\dfrac{\partial \theta}{\partial \xi} + \dfrac{\partial \varphi_i}{\partial z}\dfrac{\partial z}{\partial \xi} \\ \dfrac{\partial \varphi_i}{\partial \eta} = \dfrac{\partial \varphi_i}{\partial \theta}\dfrac{\partial \theta}{\partial \eta} + \dfrac{\partial \varphi_i}{\partial z}\dfrac{\partial z}{\partial \eta} \end{cases}$$

In its matrix form, above equation can be written as:

$$\begin{bmatrix} \dfrac{\partial \varphi_i}{\partial \xi} \\ \dfrac{\partial \varphi_i}{\partial \eta} \end{bmatrix} = \begin{bmatrix} \dfrac{\partial \theta}{\partial \xi} & \dfrac{\partial z}{\partial \xi} \\ \dfrac{\partial \theta}{\partial \eta} & \dfrac{\partial z}{\partial \eta} \end{bmatrix} \begin{bmatrix} \dfrac{\partial \varphi_i}{\partial \theta} \\ \dfrac{\partial \varphi_i}{\partial z} \end{bmatrix} \tag{3.4}$$

in which $\begin{bmatrix} \dfrac{\partial \theta}{\partial \xi} & \dfrac{\partial z}{\partial \xi} \\ \dfrac{\partial \theta}{\partial \eta} & \dfrac{\partial z}{\partial \eta} \end{bmatrix}$ is the Jacobian matrix J.

Because this transformation is reversible, there is a J^{-1} that is the inverse of J, so:

$$\begin{bmatrix} \dfrac{\partial \varphi_i}{\partial \theta} \\ \dfrac{\partial \varphi_i}{\partial z} \end{bmatrix} = J^{-1} \begin{bmatrix} \dfrac{\partial \varphi_i}{\partial \xi} \\ \dfrac{\partial \varphi_i}{\partial \eta} \end{bmatrix} \tag{3.5}$$

where $J^{-1} = \dfrac{1}{|J|} \begin{bmatrix} \dfrac{\partial z}{\partial \eta} & -\dfrac{\partial z}{\partial \xi} \\ -\dfrac{\partial \theta}{\partial \eta} & \dfrac{\partial \theta}{\partial \xi} \end{bmatrix}$ and $|J| = (\dfrac{\partial \theta}{\partial \xi}\dfrac{\partial z}{\partial \eta} - \dfrac{\partial z}{\partial \xi}\dfrac{\partial \theta}{\partial \eta})$.

Finally, the Gaussian quadrature is the numerical integration method applied to solve the integrals from -1 to 1. It states that, for a function $f(x)$ (BURDEN; FAIRES, 2010):

$$\int_{-1}^{1} f(x)dx \approx f\left(\dfrac{-\sqrt{3}}{3}\right) + f\left(\dfrac{\sqrt{3}}{3}\right)$$

Now, consider the double integral of a f function, that is our case. Regardless of what is being integrated, if either φ_i or $\varphi_i\varphi_j$:

$$\int_{\Omega_b} f(\xi, \eta)d\Omega_b = \int_{-1}^{1}\int_{-1}^{1} f(\xi, \eta)d\xi d\eta \approx$$
$$f\left(-\dfrac{\sqrt{3}}{3}, -\dfrac{\sqrt{3}}{3}\right) + f\left(\dfrac{\sqrt{3}}{3}, -\dfrac{\sqrt{3}}{3}\right) + f\left(-\dfrac{\sqrt{3}}{3}, \dfrac{\sqrt{3}}{3}\right) + f\left(\dfrac{\sqrt{3}}{3}, \dfrac{\sqrt{3}}{3}\right) \tag{3.6}$$

4 NUMERICAL ANALYSIS

The results presented in this chapter were obtained using an original code written in Python language. This code is available at <https://github.com/flaviorangel/ross-finite-element> for free access and use. Two aspects were measured in this numerical analysis for both methods: how quickly the grid converges and how much time it takes to return the pressure matrix. It is important to notice the program was run in an ordinary notebook (2.50 GHz processor, 8 GB of Random Access Memory).

4.1 PROGRAM VALIDATION

As a means to perform a validation test, i.e., make sure the program is working as it is supposed to, two checks were made for situations we know the exact result.

First, a short bearing with a rotor that is not rotating ($W = 0$) and zero pressure at both ends ($P_{in} = P_{out} = 0$) is expected to have zero pressure in all its extension, regardless of eccentricity. This situation was tested and the results came as expected.

Second, a bearing with no eccentricity and input pressure greater than output pressure ($P_{in} > P_{out}$) is expected to have its pressure decreasing linearly from $z = 0$ to $z = L$ and not varying along θ. Such test was made for the bearing specifications presented in Table 3.

Table 3 – Zero eccentricity validation test data

N_Z	Mesh points in axial direction	128
N_θ	Mesh points in azimuthal direction	128
R_o	Radius of the outer cylinder	1.000194564 m
R_i	Radius of the inner cylinder	1.0 m
ω	Angular frequency	$100\frac{2\pi}{60}$ rad/s
P_{in}	Pressure that enters the bearing	60 Pa
P_{out}	Pressure that leaves the bearing	50 Pa
L	Length of the bearing	$16R_o$
ρ	The fluid's density	860 kg/m³
μ	Fluid viscosity	0.015 Pa.s
e	The eccentricity	0.0001 m

where e is the distance between the stator's and rotor's centers. This data was based on ROSS's test for long bearing, changing only input and output pressure as well as N_Z and N_θ to better visualize.

The results of this test can be seen in Fig. 7. As expected, pressure begins at 60 Pa and linearly decreases to 50 Pa, while not varying along the azimuth axis.

Figure 7 – 3D plot of zero eccentricity validation test
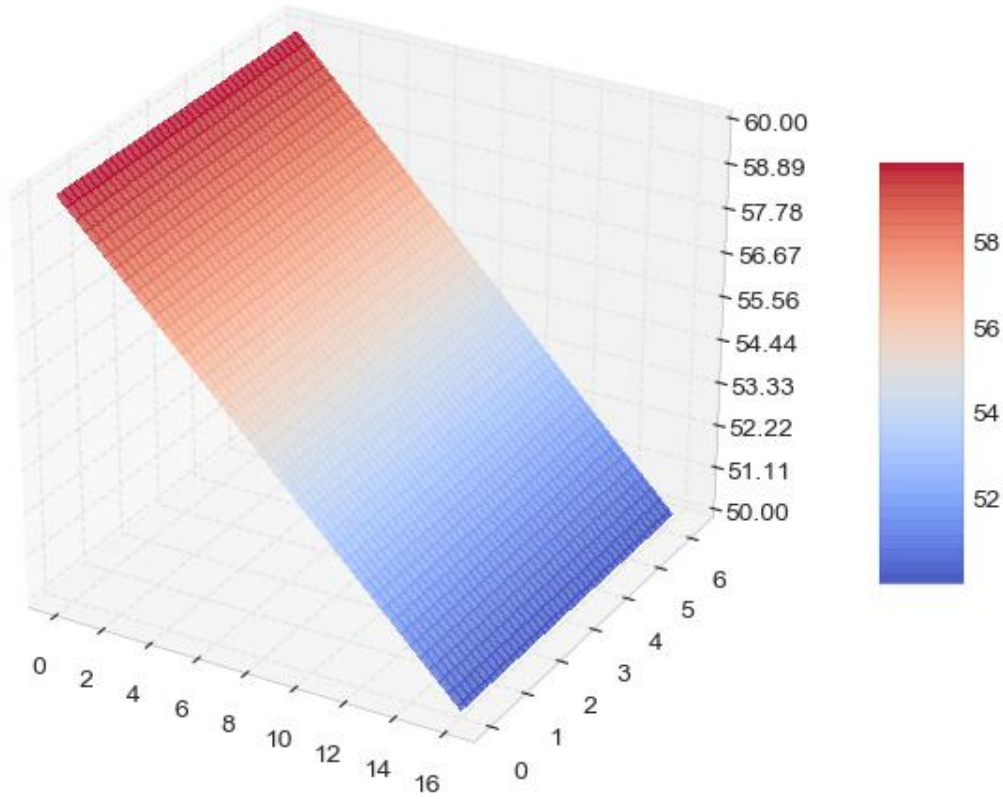
4.2 REFERENCE EXPRESSION FOR PRESSURE

With controlled error, in certain situations, the pressure inside a bearing can be calculated directly using an expression instead of a numerical method. Frene et al. (1990) do so by neglecting the axial flow in long bearings, assuming the flow to be purely circumferential, which means neglecting the second term on the left-hand side of Eq. 2.17. They assume long bearings to be those in which the ratio between their length and diameter is larger than 4, i.e., $\frac{L}{2R_o} > 4$. In a similar manner, when this same ratio is small, assumed by Frene et al. (1990) as being smaller than 1/8, then the first term on the left-hand side of Eq. 2.17 can be neglected instead.

Expressions for the pressure inside long and short bearings were used as reference for the numerical pressure calculation in this work. Based on Frene et al. (1990), the expression for short bearings is given by Eq. 4.1 and, based on Hamrock (1991), the expression for long ones is given by Eq. 4.2. The references were chosen based on the ones used by ROSS's tests to compare its own results:

$$p(\theta, z) = -\frac{3\mu\omega}{c^2}\left(z^2 - \frac{L^2}{4}\right)\frac{\varepsilon \sin\theta}{(1 + \varepsilon \cos\theta)^3} \tag{4.1}$$

$$p(\theta, z) = \frac{6\mu\omega \left(\dfrac{R_i}{c}\right)^2 \varepsilon \sin\theta \left(2 + \varepsilon\cos\theta\right)}{\left(2 + \varepsilon^2\right)\left(1 + \varepsilon\cos\theta\right)^2} + P_{in} \qquad (4.2)$$

in which c is the radial clearance, given by $c = R_o - R_i$, and ε is the eccentricity ratio, given by $\varepsilon = \dfrac{e}{c}$.

4.3   GRID CONVERGENCE

The grid convergence, executed for both the finite-difference method and the finite-element method, compares their error at maximum pressure, based on Eqs. 4.1 and 4.2, as well as the amount of time spent to calculate the pressure matrix when varying N_θ and N_Z. The following graphics (Figures from 8 to 11) represent these comparisons. The plots where obtained using Python's matplotlib package[1]. The specifications for short and long bearings are presented in Tables 4 and 5, respectively. Again, they were based on the same data used in ROSS's tests.

Two observations must be made. Firstly, as the pressure along θ-axis matters more than the one along z-axis, N_θ was increased exponentially, whereas N_Z was increased linearly. Secondly, it was not possible to calculate grids with N_θ larger than 512 due to hardware limitations.

Table 4 – Short bearing grid convergence data

|		
R_o	Radius of the outer cylinder	0.200194164 m
R_i	Radius of the inner cylinder	0.1999996 m
ω	Angular frequency	$100\frac{2\pi}{60}$ rad/s
P_{in}	Pressure that enters the bearing	0 Pa
P_{out}	Pressure that leaves the bearing	0 Pa
L	Length of the bearing	$2R_o/10$
ρ	The fluid's density	860 kg/m³
μ	Fluid viscosity	0.015 Pa.s
e	The eccentricity	0.0001 m

In practical bearings with zero pressure at both edges, the pressure in the zone from $\theta = \pi$ to 2π is almost equal to the atmospheric pressure, i.e., equal to zero. Therefore, the negative pressure that would occur is set to zero; this is the so called Gumbel condition (ISHIDA; YAMAMOTO, 2012). As pointed out by Ishida and Yamamoto (2012), the negative pressure does not occur because the fluid at such low pressure actually evaporates. This phenomenon is known as cavitation.

Two plots were made to check the pressure along θ-axis in the lowest error situation for the finite-element method, comparing with the reference expression. The error was

---

[1]   <https://matplotlib.org/>

Table 5 – Long bearing grid convergence data

R_o	Radius of the outer cylinder	1.000194564 m
R_i	Radius of the inner cylinder	1.0 m
ω	Angular frequency	$100\frac{2\pi}{60}$ rad/s
P_{in}	Pressure that enters the bearing	1 Pa
P_{out}	Pressure that leaves the bearing	0 Pa
L	Length of the bearing	$16R_o$
ρ	The fluid's density	860 kg/m³
μ	Fluid viscosity	0.015 Pa.s
e	The eccentricity	0.0001 m

Figure 8 – Short bearing comparison in N_θ
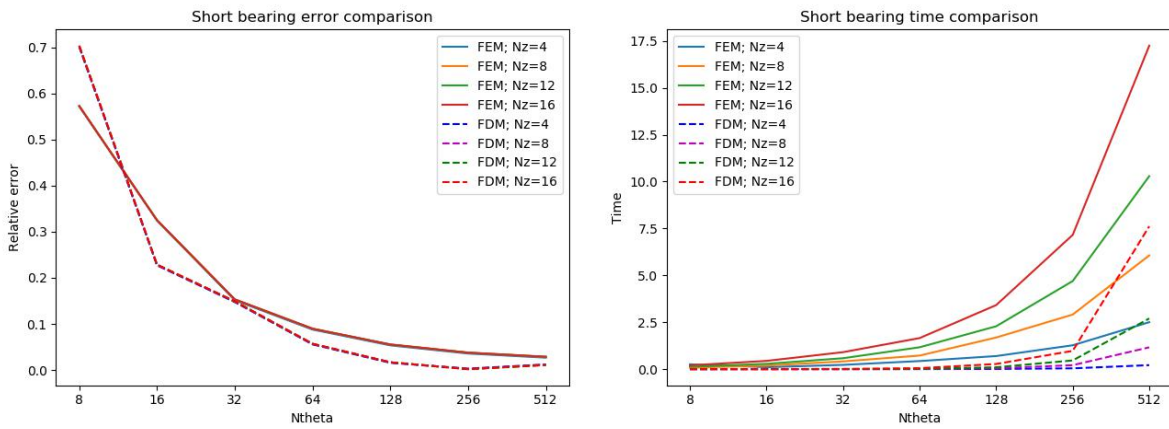
Figure 9 – Long bearing comparison in N_θ
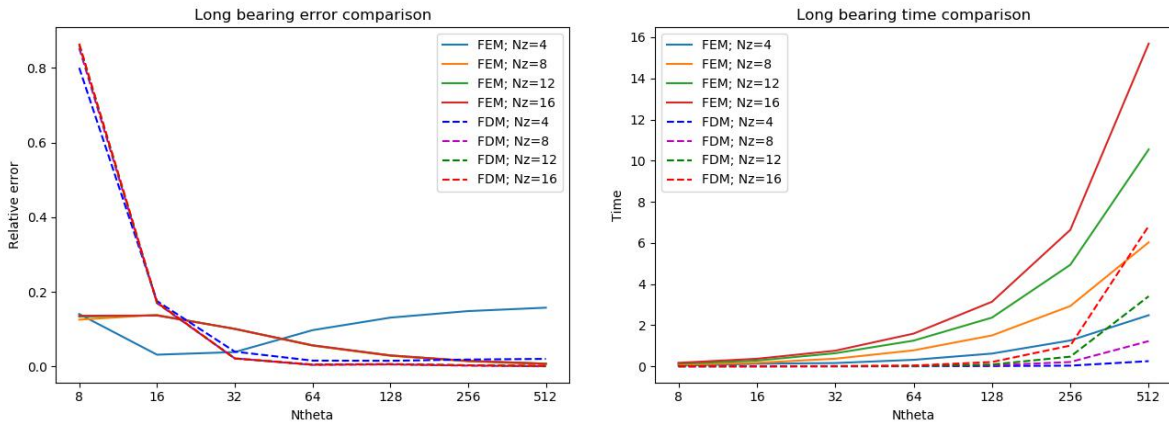
calculated based on the maximum pressure along the θ-axis, in the middle of the bearing, compared with the pressure at the same position in the numerical methods. Fig. 12 shows the pressure for short and long bearing in their middle section.

As expected, the number of mesh points in the θ-axis poses a greater impact over the grid convergence, even on the long bearing case, as can be seen in Figs. 8, 9, 10, and 11. As for the time spent, it does not vary greatly according to bearing length, since no more
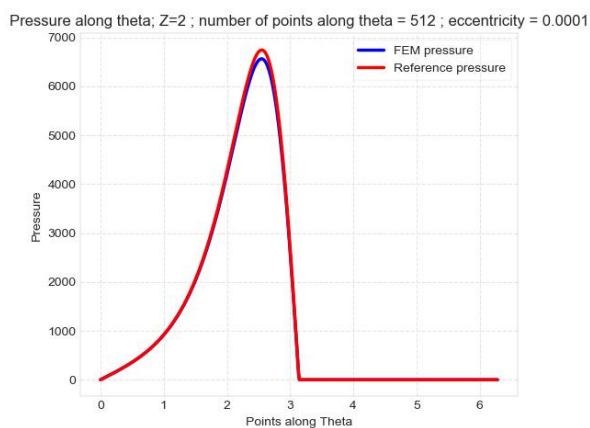
Figure 10 – Short bearing comparison in N_Z
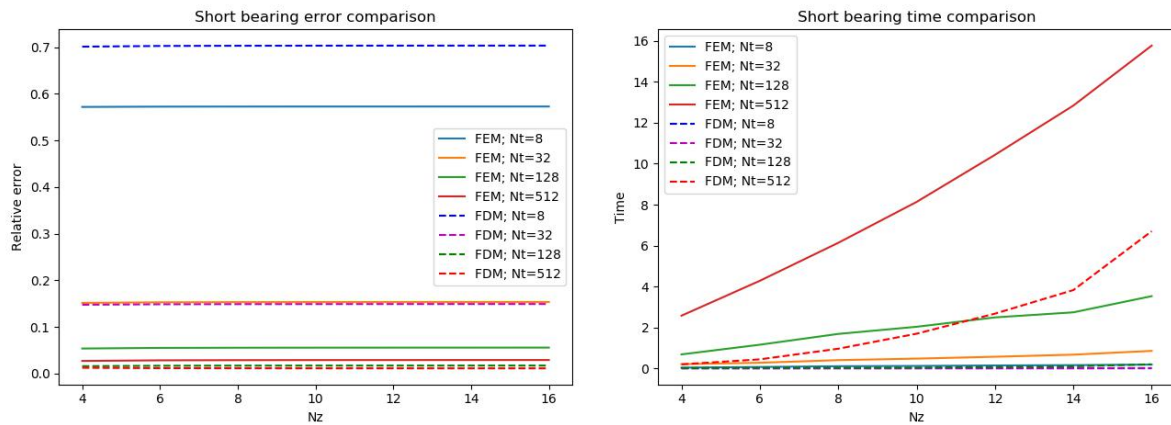
Figure 11 – Long bearing comparison in N_Z
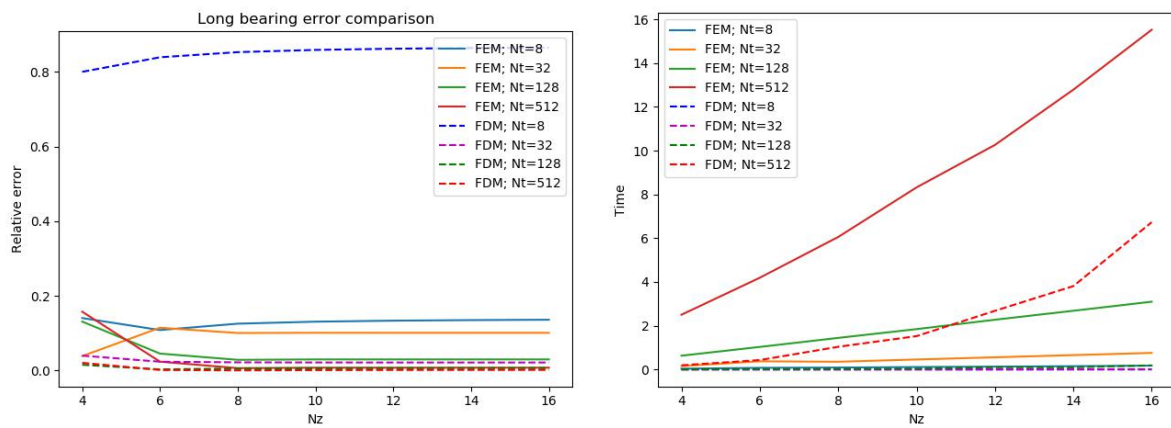
operations are added to the code, but according to number of nodes instead.

As the results show, except for a few situations, both methods converge similarly, with the finite-difference method presenting a slightly smaller error. The amount of time spent increases faster with the finite-element method. Even though in most cases it behaves similarly with the finite-difference method, it is clear that the cases in which N_θ is 512 the time spent on the finite-element method is greater.

Figure 12 – Pressure along theta for lowest error

(a) Best FEM short bearing   (b) Best FEM long bearing
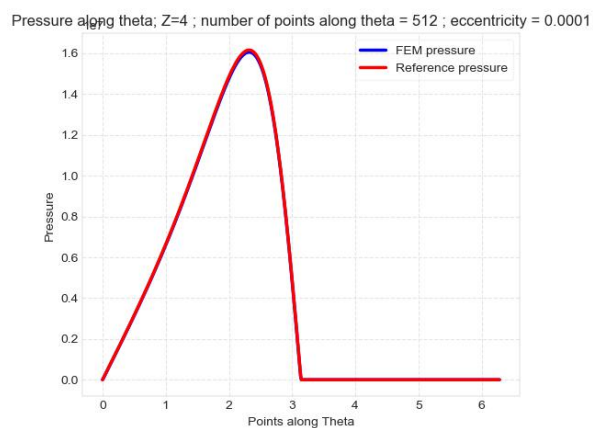
5 CONCLUSION

This work aimed to explore the use of the finite-element method instead of the finite-difference method to solve the pressure field inside the bearing, comparing and analyzing both approaches. It was possible to conclude that both methods behave similarly to solve the problem presented, but the finite-difference method performed slightly better than the finite-element method in all cases, both in terms of error and time consumption.

It is important to notice that a simple square element was applied and no irregular shaping of the boundary nor of the grid itself was present, thus most of the method's advantages were not explored. This way, the approach nearly matches the one of the finite-difference method, as the grid built is the same. Because the finite-element method is more laborious to program in comparison with the finite-difference method, specially when programmed from scratch, the finite-difference method is a more suitable choice. Regardless, the challenges involved when dealing with finite-elements do count for educational purposes.

Possible future work should involve comparing both methods for different geometries of the rotor, which would allow the use of the method's advantages. Finally, another possibility is to implement and use different types of finite elements to see which ones perform best.

BIBLIOGRAPHY

ANDRADE, S. F. A. **Asymptotic Model for Monophasic Flow Through Progressive Cavities Pump**. Dissertação (Mechanical Engineering) — Department of Mechanical Engineering of the Pontifical Catholic University of Rio de Janeiro, Rio de Janeiro, 2008.

BURDEN, R. L.; FAIRES, J. D. **Numerical Analysis**. 9. ed. Boston: Cengage Learning, 2010.

CARVALHO, M. da S.; VALÉRIO, J. **Introdução ao Método de Elementos Finitos: Aplicação em Dinâmica dos Fluidos**. São Carlos: Sociedade Brasileira de Matemática Aplicada e Computacional, 2012.

FOX, R. W.; PRITCHARD, P. J.; MCDONALD, A. T. **Fox and McDonald's introduction to fluid mechanics**. 8. ed. Hoboken: John Wiley & Sons Inc., 2011.

FRÊNE, J. et al. (Ed.). **Hydrodynamic Lubrication - Bearings and Thrust Bearings**. Amsterdan: Elsevier, 1990. v. 33. (Tribology Series, v. 33).

FRISWELL, M. et al. **Dynamics of rotating machines**. New York: Cambridge University Press, 2010.

HAMROCK, B. J. **Fundamentals of fluid lubrication**. Washington: NASA, 1991.

ISHIDA, Y.; YAMAMOTO, T. **Linear and nonlinear rotordynamics**. Weinheim: Wiley Online Library, 2012.

MOTA, J.; VALÉRIO, J.; RANGEL, F. Simplifications of navier-stokes in journal bearing simulation. In: **Anais do XIII Encontro Acadêmico de Modelagem Computacional**. Rio de Janeiro: Laboratório Nacional de Computação Científica - LNCC/MCTIC, 2020. Submitted for publication.

PINA, E. P. de; CARVALHO, M. S. Three-dimensional flow of a newtonian liquid through an annular space with axially varying eccentricity. **Journal of Fluids Engineering**, American Society of Mechanical Engineers, v. 128, n. 2, p. 223–231, 2006.

QUEIROZ, L. H. M. **Analysis of fluid flow inside rotary machines components**. Monografia (Mechanical Engineering) — Polytechnical School of the Federal University of Rio de Janeiro, Rio de Janeiro, 2018.

RINCON, M. A.; LIU, I.-S. **Introdução ao Método de Elementos Finitos**. Rio de Janeiro: [s.n.], 2015.

TIMBÓ, R. et al. Ross - rotordynamic open source software. **Journal of Open Source Software**, 2019. Submitted.